A new anisotropic diffusion method, application to partial volume effect reduction

Olivier Salvado[a], David L. Wilson[a,b];
[a] Dept. of Biomedical Engineering, Case Western Reserve University, Cleveland, OH 44106;
[b] Dept. of Radiology , University Hospitals of Cleveland, Cleveland, OH 44106.

ABSTRACT

The partial volume effect is a significant limitation in medical imaging that results in blurring when the boundary between two structures of interest falls in the middle of a voxel. A new anisotropic diffusion method allows one to create interpolated 3D images corrected for partial volume, without enhancement of noise. After a zero-order interpolation, we apply a modified version of the anisotropic diffusion approach, wherein the diffusion coefficient becomes negative for high gradient values. As a result, the new scheme restores edges between regions that have been blurred by partial voluming, but it acts as normal anisotropic diffusion in flat regions, where it reduces noise. We add constraints to stabilize the method and model partial volume; i.e., the sum of neighboring voxels must equal the signal in the original low resolution voxel and the signal in a voxel is kept within its neighbor's limits.

The method performed well on a variety of synthetic images and MRI scans. No noticeable artifact was induced by interpolation with partial volume correction, and noise was much reduced in homogeneous regions. We validated the method using the BrainWeb project database. Partial volume effect was simulated and restored brain volumes compared to the original ones. Errors due to partial volume effect were reduced by 28% and 35% for the 5% and 0% noise cases, respectively. The method was applied to in vivo "thick" MRI carotid artery images for atherosclerosis detection. There was a remarkable increase in the delineation of the lumen of the carotid artery.

Keywords: PDE, partial volume effect, anisotropic diffusion, atherosclerosis.

INTRODUCTION

We are investigating methods to reduce the partial volume effect (PVE) in medical images, a problem across many, if not all, 3D biomedical imaging modalities. Interpolation is often performed to restore the isotropy of the data set. Sometimes the goal of interpolation is enhanced 2D visualization through multiplanar reformatting. Isotropic data greatly reduces complexity in advanced image processing methods, such as 3D registration. Interpolation is often used as a preprocessing step before segmentation, in 3D visualization techniques, and before computer aided diagnosis. When a dataset has been interpolated to obtain isotropic resolution, many voxels are still subject to partial volume effect when they contain more than one tissue type. This blurring can be readily seen at the edge between two anatomical structures. Voxels with mixture of tissues are very challenging for segmentation methods. We propose in this communication an interpolation method that significantly improves the visibility of the images and reduces PVE. Our goal is not simply visual quality improvement; but on accurate PVE reduction.

As an example application, we focus on Magnetic Resonance Imaging (MRI) of human neck for atherosclerosis characterization (Figure 1). Thick slices are taken relative to their in plane resolution. A typical resolution is 0.5mm x 0.5mm x 3mm, resulting in a voxel ratio of 1:1:6. Typically 10 images are acquired transverse to the long axis of the carotid arteries. Radiologists study multiple MR contrasts to detect atheroma at the carotid bifurcation (e.g. T1W, T2W, and PDW). The anatomical dimensions of the blood vessels and the plaque features are small compared to the voxel size and multiple tissue types, i.e. multiple signal intensities, can be present in a single voxel. The result is blurring and pixelation known as partial volume effect, especially when seen in coronal or sagittal orientation (see Figure 7 for example).

Medical Imaging 2006: Image Processing, edited by Joseph M. Reinhardt, Josien P. W. Pluim,
Proc. of SPIE Vol. 6144, 614464, (2006) · 0277-786X/06/$15 · doi: 10.1117/12.649098

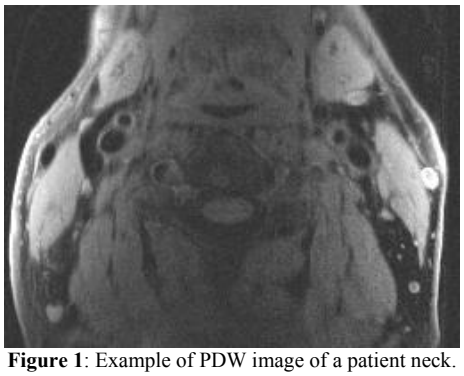

Figure 1: Example of PDW image of a patient neck.

Zero filled k-space, sinc approximations, linear and cubic interpolation are traditionally used to interpolate 3D data set. Numerous studies have shown the strengths and weaknesses of these, and more advanced algorithms. They all assume the data to be band limited and seek optimal trade off between ringing artifact and blurring. As shown in Figures 6 and 7, significant blurring is present following tri-cubic interpolation.

Classification methods exist that enable partial volume correction of areas and volumes. These methods model the image histogram, often as a Gaussian mixture, and use spatial information between voxels to estimate the mix inside each voxel of the different [1-5]. Almost all of these methods assume that a voxel can contain at most two tissue types. The performance of these methods depends upon the accuracy of histogram modeling and often specific parameters such as the number of classes. Such methods can be used to perform measurements and create high-resolution labeled images. As far as we know, these methods have not been extended to gray-scale image interpolation.

Non linear methods have been proposed to restore blurred edges, as happens with PVE, mostly to improve the visual quality of 2D images or 3D rendering (e.g. shape based interpolation) [6-8]. In particular, diffusion based methods have been proposed to achieve super-resolution. Most of those techniques start from a blurred interpolated images (e.g. using cubic interpolation) and sharpen edges by controlling the diffusion such that homogenous regions are filtered and edges between them are enhanced [9-12]. These techniques achieve impressive visual quality enhancement but they may generate extra features, which may be a reason they are seldom used for interpolating medical images. We are working on this class of techniques. Specifically, we focus on reverse diffusion techniques because they are relatively insensitive to artifact, do not rely on data modeling, can sharpen image features and reduce noise at the same time, and, very importantly, do not change average signal intensity.

In this communication we extend our reverse diffusion algorithm [13] to 3D and incorporate a new noise reduction term. In the next section, we describe the new reverse anisotropic diffusion filter especially designed to correct PVE. The following section goes over the experimental methods, before describing the results on synthetic data as well as actual MRI.

METHOD

Anisotropic diffusion filters, introduced by Perona and Malik [14] are generally described by the following formula:

$$\frac{\partial I}{\partial t} = \mathrm{div}\left[g(\|\nabla_\sigma I\|)\nabla I \right] \qquad (1)$$

where I represent the intensity of the data, $g(.)$ the diffusion coefficient, ∇ the spatial derivative, and ∇_σ the spatial derivative of the smoothed data with a Gaussian kernel of standard deviation σ. Without loss of generality, in one dimension the following forward Euler numerical approximation is used for the divergence and the time derivative:

$$I_i^n = I_i^{n-1} + dt\left(F_{i-1}^{n-1} - F_i^{n-1}\right) \qquad (2)$$

Superscript n denotes the discrete time step, and dt is chosen to assure stability. We note F the flow of materials using the analogy that the image intensity I_i represents amount of material at the location i. F_x represents then the quantity of material moving between the location i and i+1, and is dependent on the diffusion coefficient:

$F_i = F_i(I) = g(||\nabla_\sigma I||).\nabla I = g(||\nabla_\sigma I||)(I_{x+1} - I_x)$.

The standard heat equation assumes constant diffusion coefficient: $g(u) = 1$ and is equivalent to convolving the signal I with a Gaussian kernel whose standard deviation is $\sqrt{2}n$. Diffusion by a Gaussian induces blurring by moving materials in the direction of the gradient. We would like to sharpen it by reversing this process and thus we would like to move material against the gradient, or equivalently use a negative conduction coefficient $g(u) = -1$. Doing so would generate instability after only few iterations. We proposed [15] a scheme to keep the implementation tractable. Briefly, the stability of the resulting "reverse" diffusion (RD) equation was ensured by stabilization of the signal from each voxel's neighbors, using the constraints F^{high} and F^{low}. Figure 2 shows the corresponding fluxes: $F(u) = g(u)u$.

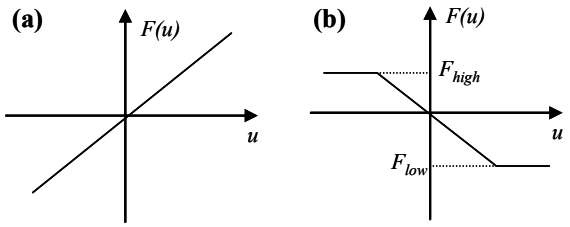

Figure 2: Flux functions for (a) standard diffusion (heat equation), and (b) reverse diffusion for two arbitrary values of the flux limits.

We now extend the approach to 3D where voxels are indexed by the letters *i*, *j* and *k*.. We use a first order explicit Euler scheme that gives the gradients and their associated fluxes in 6 directions: east, west, north, south, top and bottom. The limits for the flux (F^{high} and F^{low}) are computed at each iteration, for each voxel *ijk* as follows:

$$F_{ijk}^{high} = \underset{\{i',j',k'\}\in N_{ijk}}{\text{ord}}\left(a, I_{i'j'k'}\right) - I_{ijk} \quad (3)$$

$$F_{ijk}^{low} = I_{ijk} - \underset{\{i',j',k'\}\in N_{ijk}}{\text{ord}}\left(b, I_{i'j'k'}\right) \quad (4)$$

where $\underset{\{i',j'k'\}\in N_{ijk}}{\text{ord}}\left(n, I_{i'j'k'}\right)$ represents the n^{th} highest value over the 27 neighbor set N_{ijk}. Typical values for (a,b) are (18,10) and (17,11). The choice of (a,b) is important because it controls the trade off between resilience to noise and edge restoration. For example (1,27) is equivalent to the minimal and maximal values over the 27 neighboring and would be very sensitive to noise. The most robust to noise would be (13,15) but the flow would be very limited by its neighbors with little room for change.

Anisotropic diffusion filters use variable diffusion coefficient, and its design holds the key to the impressive performance of these filters: it should be high (strong smoothing) for low gradient, corresponding to noisy homogeneous regions of the data, and low (little smoothing) to preserve edges between regions. Recent variations suggested stopping the diffusion [16], or even forcing it to be negative to actively enhance edges [9]. We extend our reverse diffusion scheme to by incorporating such a filtering term (inspired from [14]) to smooth low SNR data while keeping its edge enhancing capability. The new diffusion coefficient and associated flux are shown in Figures 3a and 3b respectively, and correspond to

$$g(u) = \frac{(1+\alpha)}{1+(u/k)^2} - \alpha \quad (5)$$

where k defines the scale of the noise, and α the amount of reverse diffusion that we kept to unity on all the results of this paper. To ensure stability constraint from neighbors are used in the way as for the RD by using Equations (3) and (4). We refer to this new version as reverse anisotropic diffusion (RAD).

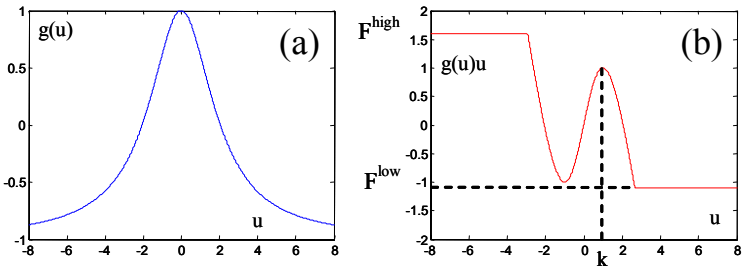

Figure 3: Reverse anisotropic diffusion coefficient (a) and flux (b) for two arbitrary values of the flux limits.

In addition, we assume that PVE can be modeled as the integral of the signal over the volume of a voxel. That is to say that if we split a voxel into sub-voxels (interpolation) the sum of the sub-voxels should always be equal to the original voxel value. A direct consequence is the constraint that the fluxes should be zero at voxel boundaries (but not at sub-voxel ones). We refer to this boundary constraint as BC.

We correct a data set as follows. First, voxel data are interpolated with nearest neighbor by duplicating each voxel to obtain the desired resolution. For example to increase the overall resolution by two, each voxel is split into 8 sub-voxels. Second, RD and/or RAD filters are run on the oversampled data set while constraining the flow to be zero at the original voxel boundaries using BC.

3. EXPERIMENTAL METHOD

The quantitative validation of our method requires obtaining both a high and low resolution data set. Correction of the low resolution volume would then be compared to the high resolution one, the "ground truth". However, it is very difficult to obtain two such data sets because of slight differences in the acquisition and different noises. We therefore used simulation data. Because our method could be applied advantageously to brain MRI, we used the validation data set from the BrainWeb project [17]. We used the simulated images with the highest resolution: 1mm×1mm×1mm. We then simulated PVE by averaging several voxels into one to yield a low resolution volume that we interpolated with our method. We could then compare results to the original high resolution data. We tested the robustness to noise by adding Gaussian noise whose standard deviation was expressed as a percentage of the dynamic range. The performance was computed using the root mean square error between the original high resolution volume and the corrected volumes. The results of our method were compared to ones obtained by tri-cubic interpolation of the low resolution volume.

The method was also applied to patient MRI of neck. Sixteen patients with carotid artery stenosis, as documented by duplex ultrasound, were recruited for the study. Informed consent was obtained from all subjects under a protocol approved by the institutional review board for human investigation. All MR scans were conducted on a 1.5 T system (Magnetom Sonata; Siemens, Erlangen, Germany) with a custom-built phased array coil. Dark blood images were obtained using ECG-triggered double inversion recovery (DIR) turbo spin echo sequences. Imaging parameters (TR/TE/TI/NSA/thickness/FOV) were as follows: T1W: 1R-R/7.1ms/500ms/2/3mm/13cm; PDW: 2R-R/7.1ms/600ms/2/ 3mm/13cm; T2W: 2R-R/68ms/ 600ms/2/3mm/13cm. Fat saturation was applied. The in plane resolution was $0.51\times0.51\text{mm}^2$. Original data had thus a ratio of 1:1:6 corresponding to the resolution $0.51\times0.51\times3\text{mm}^3$ and were interpolated to yield a volume with resolution 0.26mm^3. Visual quality was assessed by observing the volumes along the three common directions (axial, sagittal, and coronal).

For all cases, RD interpolation was first applied using 50 iterations, before running 5 iterations of RAD. Boundary constraints were used only for the RD step. Parameters were a=11, b=17, α=1, k=2% of dynamic range.

4. RESULTS

Figure 4, 5 and 6 show results from the synthetic T1 brain data experiments. We corrected simulated low resolution volume and interpolated back to original resolution. The table in Figure 4 shows the RMS error between the corrected data and the original high resolution. RD with BC reduced the error by 25% and 35% for the 5% and the 0% noise cases respectively. Subsequent application of RAD did not reduce the error in the noise free case, as expected, but could

reduce subsequently the error by 3%. Tri-cubic resolution reduced much less the error: 11% and 9.5% for the 5% and 0% noise respectively, and introduced strong blurring.

Figure 5 shows heavy partial volume effect corrected with the proposed method for illustration purposes. Even under those conditions, interface between tissues could be restored quite accurately. Of course, small image features were lost because of the signal dilution. This example illustrates the benefit of the method: edges between homogenous areas can be restored when possible, otherwise the signal is little changed, and no artifacts are produced. Figure 6 shows selected axial, sagittal and coronal views of the 5% case from the results in Figure 4. Interfaces between air/skull white/gray matter and CSF/gray matter were restored and matched closely those of the original dataset.

In Figure 7, we show two examples of the correction of actual patient neck MR images. Thick slices can be seen on the sagittal and coronal views. After correction with our method delineation of the lumen of the carotid artery were much sharper, and partial volume effect at the bifurcation where the common carotid artery branches into the internal and external carotid arteries was also significantly reduced in a way that seemed natural and consistent with the surrounding anatomical structures. The two examples shown here are representative of typical signal to noise ratio of such images. The corrected images are free of the heavy blurring resulting of tri-cubic interpolation typically seen in such cases.

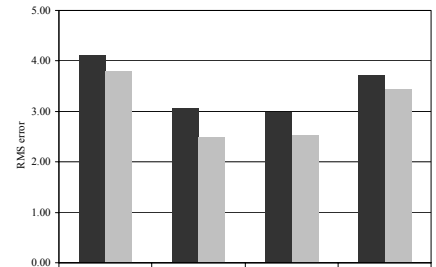

	Original	RD	RD+RAD	Tri-cubic interpolation
5% noise	4.12	3.06	2.98	3.70
no noise	3.79	2.49	2.54	3.43

Figure 4: BrainWeb phantom correction results. Partial volume effect was simulated on a Brain phantom, corrected with different methods and quantitatively compared to the original. RMS errors are shown in the 5% and 0% noise cases.

5. DISCUSSION AND CONCLUSION

The proposed method gives improved subjective image quality and truer intensities as compared to conventional interpolation schemes. The reverse diffusion method allows one to interpolate images while recovering edges which have been blurred due to the partial volume effect. With the proposed method, subjective blurring of interpolated images is reduced on synthetic brain MR images and actual neck MR images (Figures 5-7) as compared to conventional interpolation schemes. This is done without introducing artifacts. Quantitative evaluation on the synthetic images showed that the true signal intensity was recovered at edges and that the interpolated image was very close to the actual high resolution image (Figures 5 and 6).

RD followed by RAD can correct low SNR data. That is, we found that partial voluming can be reduced on simulated data even in the presence of noise (Figure 4), as well as on MR images with typical noise levels (Figure 7). RD can recover sharp edges. Because a model for PVE is used in our method, infinitely sharp edges could theoretically be fully recovered to the limit of the data resolution. In contrast, features smaller than a voxel cannot be recovered since no particular information is available to the algorithm. RD can thus be considered as a non-linear high pass filter, acting mostly for edge information and able to estimate the high frequency components of edges above the Nyquist frequency. The high frequencies in the original data higher than the Nyquist frequency that are not recovered correspond to structure smaller than a voxel size, as showed in results on our synthetic phantom (Figure 5). Satisfactorily in this latter case, the method does not change the data nor produces artifact.

In our current implementation the point spread function should be small relative to a voxel. One of our main assumptions, shared by almost all methods correcting partial volume effect [5], is that the signal is averaged over a voxel. This requires the point spread function (PSF) to be about equal or smaller than the size of a voxel at the coarse resolution, which is reasonable in MRI. If this is not the case, most of the blurring would come from the PSF convolution with the data rather than signal averaging inside the voxel. For the case of a large PSF, it would be

necessary to control the flow of materials over a spatial support corresponding to the size of the PSF rather than the original voxel.

Other methods exist to sharpen edges and smooth noise to qualitatively improve images based on non-linear diffusion. Our proposed scheme is related to some of them [9,10,18], but also uses a new way to constrain the fluxes by using voxel boundaries, and stabilize the numerical implementation using neighborhood information. The resulting algorithm is simple, robust to noise and artifacts, does not require data modeling, and can reduce substantially partial volume effect. Because of the BC, noise remains that can be noticed in homogeneous region. That led us to subsequently apply 5 iterations of the RAD filter. Because the RAD filter shares the same parameters (noise scale and neighborhood constraints), edges are mostly left unchanged but the noise in homogeneous areas can be significantly reduced.

ACKNOWLEDGMENT

This work was supported by Ohio Wright Center of Innovation and Biomedical Research and Technology Transfer award: “The Biomedical Structure, Functional and Molecular Imaging Enterprise”.

REFERENCES

1. Ruan, S., Jaggi, C., Xue, J., Fadili, J., and Bloyet, D. "Brain tissue classification of magnetic resonance images using partial volume modeling". Medical Imaging, IEEE Transactions on 19[12], 1179-1187. 2000.
2. Santago, P. and Gage, H. D. "Statistical models of partial volume effect". Image Processing, IEEE Transactions on 4[11], 1531-1540. 1995.
3. Laidlaw, D. H., Fleischer, K. W., and Barr, A. H. "Partial-volume Bayesian classification of material mixtures in MR volume data using voxel histograms". Medical Imaging, IEEE Transactions on 17[1], 74-86. 1998.
4. Choi, H. S., Haynor, D. R., and Kim, Y. "Partial volume tissue classification of multichannel magnetic resonance images-a mixel model". Medical Imaging, IEEE Transactions on 10[3], 395-407. 1991.
5. Van Leemput, K., Maes, F., Vandermeulen, D., and Suetens, P. "A unifying framework for partial volume segmentation of brain MR images". Medical Imaging, IEEE Transactions on 22[1], 105-119. 2003.
6. Ting, Hou-Chun and Hang, Hsueh Ming. "Edge Preserving Interpolation of Digital Images Using Fuzzy Inference". Journal of Visual Communication and Image Representation 8[4], 338-355. 1997.
7. Battiato, Sebastiano, Gallo, Giovanni, Mancuso, Massimo, Messina, Giuseppe, and Stanco, Filippo. "Analysis and characterization of super-resolution reconstruction methods". *5017*[*1*], 323-331. 5-14-2003. SPIE, Santa Clara, CA, USA.
8. Morigi, S. and Sgallari, F. "3D long bone reconstruction based on level sets". Computerized Medical Imaging and Graphics 28[7], 377-390. 2004.
9. Gilboa, G., Sochen, N., and Zeevi, Y. Y. "Forward-and-backward diffusion processes for adaptive image enhancement and denoising". Image Processing, IEEE Transactions on 11[7], 689-703. 2002.
10. Pollak, I., Willsky, A. S., and Krim, H. "Image segmentation and edge enhancement with stabilized inverse diffusion equations". Ieee Transactions on Image Processing 9[2], 256-266. 2000.
11. Alvarez, L. and Mazorra, L. "Signal and Image-Restoration Using Shock Filters and Anisotropic Diffusion". Siam Journal on Numerical Analysis 31[2], 590-605. 1994.
12. Remaki, L. and Cheriet, M. "Numerical schemes of shock filter models for image enhancement and restoration". Journal of Mathematical Imaging and Vision 18[2], 129-143. 2003.
13. Salvado O., Hillenbrand C., and Wilson, D. L. "Partial volume reduction by interpolation with reverse diffusion". International Journal of Biomedical Imaging . In press 2006.
14. Perona, P. and Malik, J. "Scale-space and edge detection using anisotropic diffusion". Pattern Analysis and Machine Intelligence, IEEE Transactions on 12[7], 629-639. 1990.
15. Salvado O., Hillenbrand C., and Wilson, D. L. "Partial volume correction using reverse diffusion.". *5747*, 625-633. 2005. SPIE, San Diego, CA.
16. Black, M. J., Sapiro, G., Marimont, D. H., and Heeger, D. "Robust anisotropic diffusion". Image Processing, IEEE Transactions on 7[3], 421-432. 1998.
17. Kwan, R. K. S., Evans, A. C., and Pike, G. B. "MRI simulation-based evaluation of image-processing and classification methods". Medical Imaging, IEEE Transactions on 18[11], 1085-1097. 1999.

18. Breuss, Michael, Brox, Thomas, Sonar, Thomas, and Weickert, Joachim. *Stabilised Nonlinear Inverse Diffusion for Approximating Hyperbolic PDEs*. 3459, 536-547. 2005.

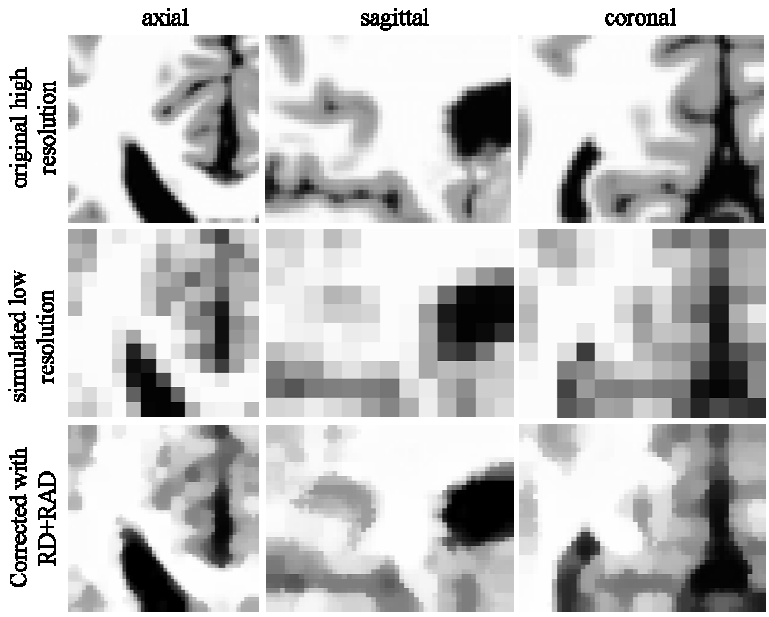

Figure 5. Heavy partial volume effect reduction. To illustrate how our proposed method work, we simulated strong partial volume effect by averaging 64 voxels of the original volume (top row) into one voxel in the simulated low resolution (middle row). The corrected volume with the proposed method is shown on the bottom row. Selected axial, sagittal, and coronal views are shown for each volume.

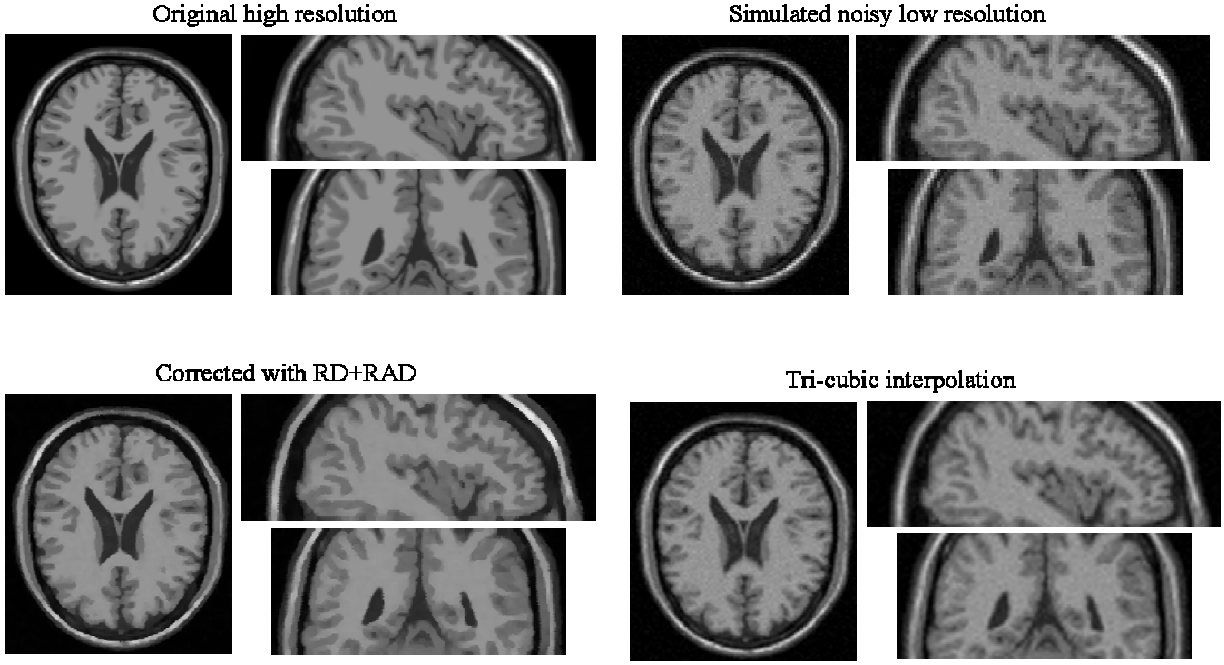

Figure 6. Correction of synthetic brain phantom. The original T1 brain phantom (top left) was dowsnampled, and noise was added to yield a low resolution volume (top right). The bottom left panel, shows the restored image with our proposed method. Bottom right shows the same result using tri-cubic interpolation. Selected axial, sagittal, and coronal views are shown for each volume.

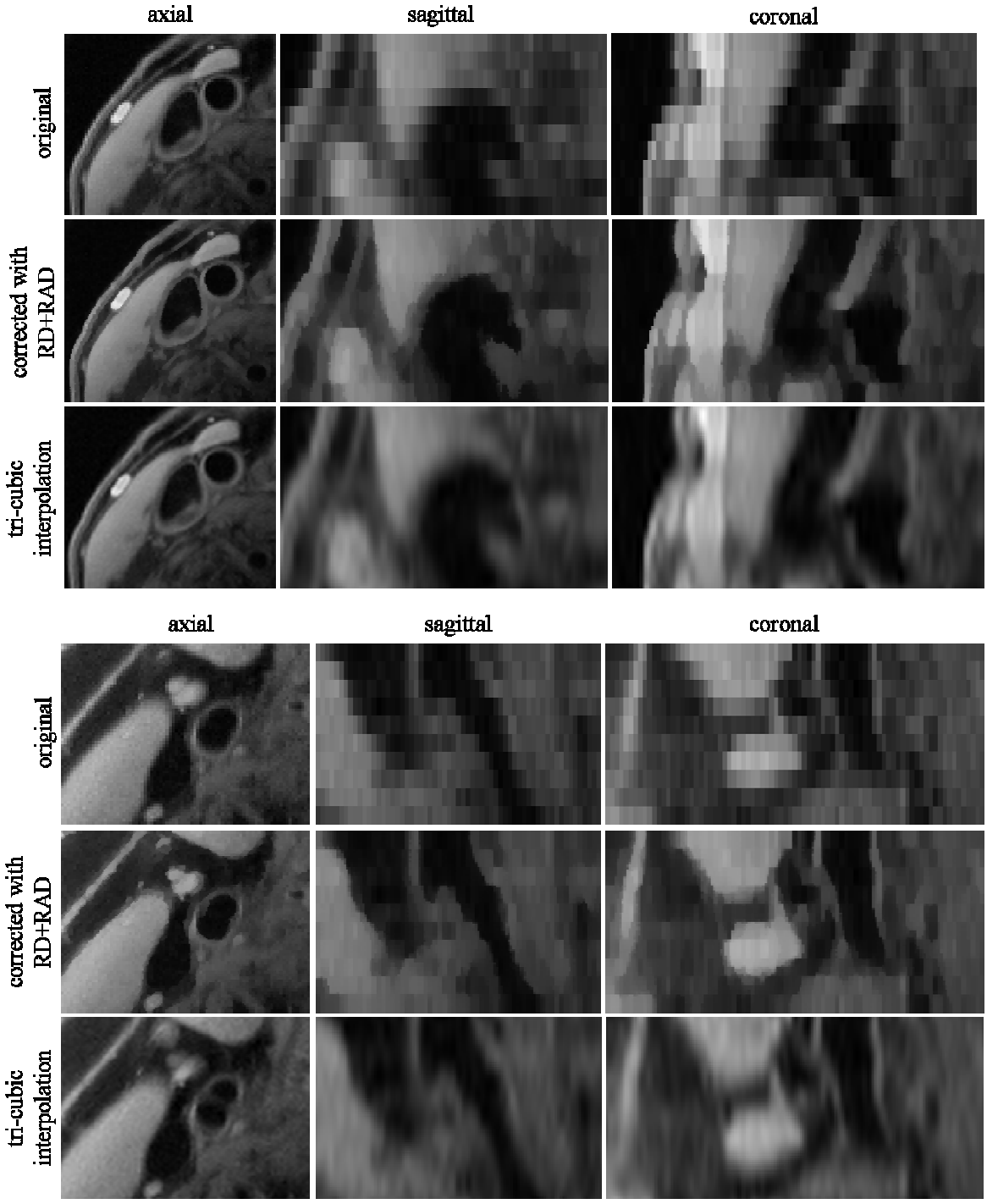

Figure 7. Correction of two PDW neck patient images. Actual MR images of patient neck acquire with thick 3mm slices and $0.51\times0.51\text{mm}^2$ inplane resolution were interpolated with our proposed method as well as tri-cubic interpolation to yield a dataset with $0.26\times0.26\times0.375\text{mm}^3$ resolution. Selected axial, sagittal, and coronal views are shown for each volume.